Monthly Notices of the Royal Astronomical Society

Mon. Not. R. Astron. Soc. (2011)

doi:10.1111/j.1365-2966.2011.19877.x

Magnetohydrodynamic simulations of flows around rotating and non-rotating axisymmetric magnetic flux concentrations

T. Hartlep,[1★] F. H. Busse,[2] N. E. Hurlburt[3] and A. G. Kosovichev[1]

[1]*W. W. Hansen Experimental Physics Laboratory, Stanford University, Stanford, CA 94305, USA*
[2]*Institute of Physics, University of Bayreuth, 95440 Bayreuth, Germany*
[3]*Lockheed Martin Solar and Astrophysics Laboratory, Palo Alto, CA 94304, USA*

Accepted 2011 September 22. Received 2011 September 16; in original form 2011 April 15

ABSTRACT

We present results on modelling magnetic flux tubes in an unstably stratified medium and the flows around them using 2D axisymmetric magnetohydrodynamic (MHD) simulations. The study is motivated by the formation of magnetic field concentrations at the solar surface in sunspots and magnetic pores and the large-scale flow patterns associated with them. The simulations provide consistent, self-maintained models of concentrated magnetic field in a convective environment, although they are not fully realistic or directly applicable to the solar case. In this paper, we explore under which conditions the associated flows near the surface are converging (towards the spot centre) or diverging (away from the axis) in nature. It is found that, depending on the parameters of the problem, the results can depend on the initial conditions, in particular for zero or low rotation rates and Prandtl numbers smaller than unity. The solutions with a converging flow generally produce more strongly confined magnetic flux tubes.

Key words: magnetic fields – MHD – methods: numerical – sunspots.

1 MOTIVATION AND OBJECTIVES

The mechanisms of how magnetic pores and sunspots form on the Sun are still poorly understood. Observations and numerical simulations suggest that their structure is intimately linked with characteristic surface and subsurface flows in and around the region of magnetic field concentration. Fully developed sunspots exhibit a surface outflow in their penumbra, the so-called Evershed flow, presumed to be caused by interaction between the near-surface granular convection and the highly inclined penumbral magnetic field as suggested by Hurlburt, Matthews & Proctor (1996) and the numerical simulations of Kitiashvili et al. (2009). Observation (e.g. Zhao, Kosovichev & Sekii 2010) have revealed downflows in the central region of the sunspot and subsurface converging flows (inflows) below the granulation layer, as well as outflows further below. The inflows around magnetic structures without penumbra were also obtained in the realistic magnetohydrodynamic (MHD) simulations of Rempel, Schüssler & Knölker (2009) and Kitiashvili et al. (2010). On the other hand, the simulations of Rempel (2011) found outflows even below the Evershed flow. Either way, it is conjectured that the structure of the flow plays a fundamental role for maintaining the integrity of the magnetic field concentration.

These problems are the motivation for the present study. As impressive and sophisticated as the best current numerical simulations are, they still are not fully realistic, and as in the case of Rempel (2011) rely on specialized boundary conditions to hold the magnetic field in place and keep it from dispersing. In this study, instead of trying to improve on these high-fidelity simulations, we chose to study the problem in a more simplified setting that still captures important aspects of the physics. We study the subsurface magnetoconvection of magnetic flux concentrations in an axisymmetric configuration and model convection in a parametrized way. The transport coefficients used here do not describe the molecular transport, but rather can be thought of as the aggregate effect of the small-scale flow that is not modelled here. We specifically exclude the complicated convection at the photosphere (where the Evershed flow forms in penumbrae), which is primarily driven by radiation effects. In our approach, many small-scale details will be lost and quantitative comparisons with the actual Sun may be difficult. None the less, this provides us with a tool for studying the qualitative behaviour and whether inflows are necessary to keep magnetic structures confined. Similar simulations by Hurlburt & Rucklidge (2000), Botha, Rucklidge & Hurlburt (2006) and Botha et al. (2008) have been able to reproduce flow structures similar to those discussed above, and Botha et al. (2008) did, for instance, find magnetic flux concentrations with both diverging surface flow over a converging flow and vice versa. The present paper extends their work, exploring in more detail the conditions under which diverging or converging flows can hold a magnetic flux concentration in place.

★E-mail: thartlep@stanford.edu

2 NUMERICAL METHOD

We study magnetoconvection in an axisymmetric cylindrical geometry using a code originally developed by Hurlburt & Rucklidge (2000) for the 2D case and later extended by Botha et al. (2008) to include azimuthal components of velocity and magnetic fields. The model considers a layer of electrically conducting, perfect monatomic gas subject to uniform gravitational acceleration, with constant shear viscosity, magnetic diffusivity and magnetic permeability, rotating with constant angular velocity Ω about the vertical. The model approximates the conditions in the upper part of the solar convection zone but excludes the granulation layer, the very top few hundred kilometres below the photosphere where the plasma is only partially ionized and radiation would need to be modelled accurately.

The equations in non-dimensional form read

$$\partial_t \rho = -\nabla \cdot (\boldsymbol{u}\rho), \tag{1}$$

$$\begin{aligned}\partial_t \boldsymbol{u} = &-\boldsymbol{u}\cdot\nabla\boldsymbol{u} - 2\Omega\hat{z}\times\boldsymbol{u} + \Omega^2(\hat{z}\times\boldsymbol{r})\times\hat{z} \\ &-\frac{1}{\rho}\nabla P + \theta(m+1)\hat{z} \\ &+\frac{\sigma K}{\rho}\nabla\cdot\tau + \frac{\sigma K^2 Q\zeta_0}{\rho}\boldsymbol{j}\times\boldsymbol{B},\end{aligned} \tag{2}$$

$$\begin{aligned}\partial_t T = &-\boldsymbol{u}\cdot\nabla T - (\gamma-1)T\nabla\cdot\boldsymbol{u} + \frac{\gamma K}{\rho}\nabla^2 T \\ &+\frac{\sigma K(\gamma-1)}{\rho}\left(\frac{1}{2}\tau:\tau + \zeta_0^2 Q K^2 j^2\right),\end{aligned} \tag{3}$$

$$\partial_t A_\phi = (\boldsymbol{u}\times\boldsymbol{B})_\phi - \zeta_0 K j_\phi, \tag{4}$$

$$\partial_t B_\phi = [\nabla\times(\boldsymbol{u}\times\boldsymbol{B})]_\phi + \zeta_0 K\left(\nabla^2 B_\phi - \frac{B_\phi}{r^2}\right), \tag{5}$$

where ρ, T, $\boldsymbol{u}$ and $\boldsymbol{B}$ are the density, temperature, velocity and magnetic field, $\boldsymbol{B} = \nabla\times(\hat{\boldsymbol{\phi}}A_\phi) + \hat{\boldsymbol{\phi}}B_\phi$, respectively. $\boldsymbol{j}$ and τ stand for the current density and the rate of strain tensor. We have used cylindrical coordinates with $\hat{z}$ being the vertical direction pointing downwards, $\hat{\boldsymbol{r}}$ being the radial direction and $\hat{\boldsymbol{\phi}}$ the azimuthal direction. The quantities are non-dimensionlized using the depth d of the domain as a scale for length, the sound speed at the top of the domain as a scale for velocities, and initial temperature, density, pressure and magnetic field at the top of the domain as scales for their respective quantities. The equations are solved numerically using a finite-difference scheme accurate to sixth-order and a fourth-order time marching scheme.

The control parameters in the simulation are the Rayleigh number at the mid-plane, R, defined as

$$R = \theta^2(m+1)\left[1 - \frac{(m+1)(\gamma-1)}{\gamma}\right]\frac{(1+\theta/2)^{2m-1}}{\sigma K^2}; \tag{6}$$

the Prandtl number, σ; the temperature contrast between the top and the bottom of the domain, θ; the rotation rate, Ω; the aspect ratio, the ratio between height and radius of the cylindrical domain, Γ; and the Chandrasekhar number, Q, a measure of the magnetic flux in the system defined as

$$Q = \frac{(B_0 d)^2}{\mu\rho\eta\nu}, \tag{7}$$

where μ, η, ν and B_0 are the magnetic permeability, magnetic diffusivity, kinematic viscosity and the scale of the initial magnetic field, respectively. The ratio between specific heats is chosen to be $\gamma = 5/3$, appropriate for a monoatomic ideal gas. The initial temperature and density profiles in the simulations take the form of a polytrope, in non-dimensional form $T(z) = 1 + \theta z$, $\rho(z) = (1 + \theta z)^m$, where z and m are the non-dimensional depth (ranging from 0 at the top of the domain to 1 at the bottom) and the polytropic index, respectively. Simulations are started with an initial uniform vertical magnetic field $\boldsymbol{B} = \hat{z}$ (in non-dimensional units), and are run until the system reaches steady state, if such a state can be obtained for the given set of parameters.

For thermal boundary conditions, we prescribe a constant heat flux at the bottom and Stefans law at the top. The side wall is perfectly electrically conducting and does not allow for a heat flux across it. Top, bottom and outside walls are impenetrable and stress free. The magnetic field is vertical at the bottom and matched to a potential field at the top. The results presented in this paper are for aspect ratio $\Gamma = 3$.

3 RESULTS

This work is an extension of Botha et al. (2006 ,2008), in which we are exploring under which conditions a stable magnetic flux concentration forms with an outflow (away from the centre) over an inflow or vice versa. Unless otherwise specified, the simulation parameters for the results presented here are $Q = 32$, $m = 1$, $\Gamma = 3$, $\zeta_0 = 0.2$, $\Omega = 0.1$, $\sigma = 1$, $\theta = 10$ and $R = 10^5$, referred to as the reference case in the text below. This is a case in which a diverging (away from the rotation axis) over a converging flow forms. Simulation results for the same parameters were originally presented in fig. 17 of Botha et al. (2008). In both cases, a small converging flow was prescribed as initial condition. A visualization of the flow and the magnetic field is shown here in Fig. 1. Note that the magnetic field is confined to the region near the axis where the convection flow is mostly suppressed. A stationary diverging flow exists outside of the strong magnetic field region.

Starting from this reference case, we performed a parameter study varying Prandtl number, rotation rate and, for a limited number of cases, the Chandrasekhar number. We have found that in many cases the initial conditions are important. For most parameter sets we therefore performed both a simulation with a weak converging circulation (flow towards the rotation axis near the top boundary and away from the axis below) and with a weak diverging flow as initial conditions. The resulting flow configurations for Chandrasekhar number $Q = 32$ and varying Prandtl number and rotation rate are presented in Table 1. The resulting configurations are classified as either a well confined flux tube with a diverging flow at the top, a flux tube with a converging flow near top, or as not well

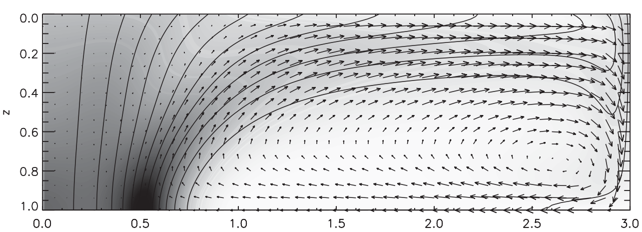

Figure 1. Flow velocities (arrows), magnetic field strength (grey-scale, with dark indicating stronger magnetic field) and magnetic field lines for the reference case, a case that forms a diverging flow over a converging flow. See text for parameters. The rotation axis is on the left at $r = 0$.

Table 1. Resulting flow configurations as a function of Prandtl number σ and rotation rate Ω. C: well-confined magnetic flux concentration with a converging flow around it; D: a well-confined magnetic flux concentration with a diverging flow around it; and X: a configuration with poor confinement of the magnetic field according to the criterion described in the text, respectively. The top part of the table is for the cases with an initial weak converging flow, and the bottom part is for an initially diverging flow. The other simulation parameters in all cases are $Q = 32$, $R = 10^5$, $\theta = 10$, $\gamma = 5/3$, $m = 1$, $\zeta_0 = 0.2$ and $\Gamma = 3$.

Converging flow initial condition:		Prandtl number σ			
		0.1	0.3	1.0	2.0
Rotation rate Ω	0.00	C	C	C	D
	0.02	C	C	D	D
	0.05	C	C	D	D
	0.10	C	D	D	D
Diverging flow initial condition:		**Prandtl number σ**			
		0.03	0.1	0.3	1.0
Rotation rate Ω	0.00	X	D	D	D
	0.02	X	D	D	D
	0.05	X	D	D	D
	0.10	X	X	D	D

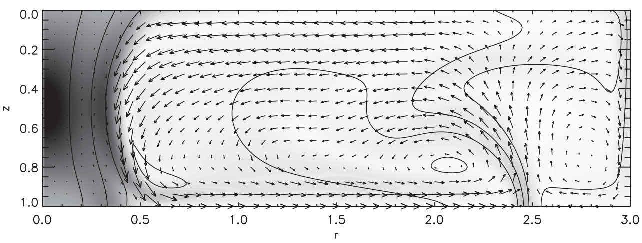

Figure 2. Same parameters as the reference case (Fig. 1) except for $\theta = 20$ and $R = 4 \times 10^5$.

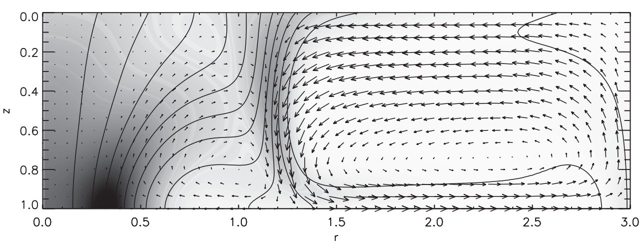

Figure 3. Same parameters as the reference case (Fig. 1) except for rotation rate $\Omega = 0$.

confined. Examples for these three cases are shown in Figs 1, 2 and 3, respectively.

Of course, the definition of what is a well-confined magnetic structure is somewhat arbitrary. Here, we used the following quantitative definition to determine the diameter of the magnetic field concentration around the centre of the domain at the top boundary:

$$D = 2\sqrt{2\log 2 \frac{\int_0^{r_l} \|\boldsymbol{B}(z=0,r)\| r^2 \,\mathrm{d}r}{\int_0^{r_l} \|\boldsymbol{B}(z=0,r)\| \mathrm{d}r}}, \tag{8}$$

where r_l is the smallest radius that fulfils the condition:

$$\|\boldsymbol{B}(z=0,r_l)\| < \frac{5}{100} \max_{r<r_l} \|\boldsymbol{B}(z=0,r)\|. \tag{9}$$

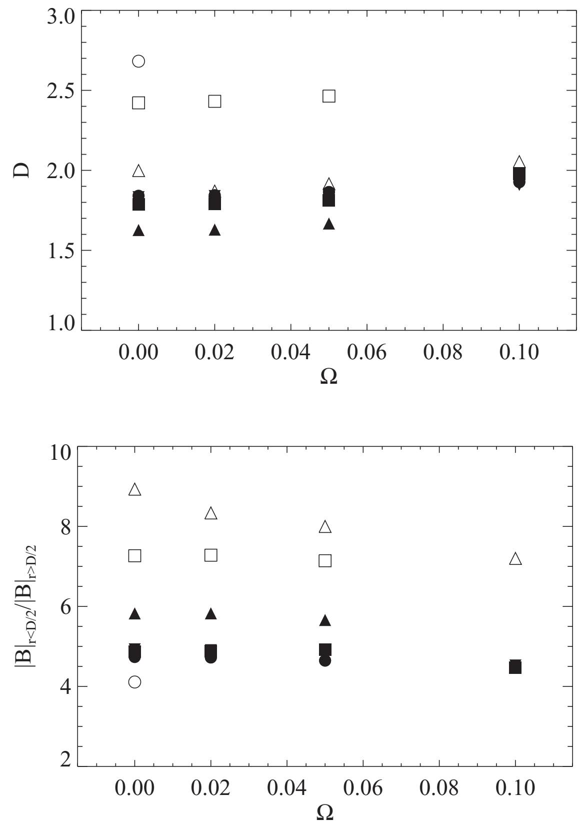

Figure 4. Horizontal diameter, D, of the magnetic field concentration (top panel) and ratio between mean magnetic field strength inside the field concentration and outside (bottom panel) as a function of the rotation rate Ω. The symbols correspond to Prandtl number 0.03 (diamonds), 0.1 (upward triangles), 0.3 (squares), 1.0 (circles) and 2.0 (downward triangles). Open symbols are for resulting converging flows and solid symbols for diverging flows, respectively.

This conditions makes sure that only the innermost magnetic structure is taken into account in cases where there is additional magnetic field somewhere outside. The threshold of 5/100 is quite arbitrary but seems to work well for our purposes. We then compute the average magnetic field inside the radius $r \leqslant D/2$ and outside:

$$|B|_{r<D/2} = \int_0^{D/2} \|\boldsymbol{B}(z=0,r)\| r \mathrm{d}r \Big/ \int_{D/2}^{\Gamma} r \mathrm{d}r, \tag{10}$$

$$|B|_{r>D/2} = \int_{D/2}^{\Gamma} \|\boldsymbol{B}(z=0,r)\| r \mathrm{d}r \Big/ \int_{D/2}^{\Gamma} r \mathrm{d}r. \tag{11}$$

We consider the magnetic field region as well confined if the ratio $|B|_{r<D/2}/|B|_{r>D/2}$ is larger than 4, meaning the magnetic field inside the region is at least four times larger than the ambient field outside. Both quantities, the field strength ratio and the diameter, are plotted in Figs 4 and 5 for the cases forming well-confined magnetic structures.

The results in Table 1 show that diverging flow configurations are preferred at higher values of the rotation rate as well as of the Prandtl number. At lower Prandtl numbers and/or lower rotation rate, the results depend on the initial conditions, i.e. the resulting flow is diverging if a weak diverging flow was prescribed as initial condition and vice versa. Of course, the strength and size of the magnetic field concentration varies depending on the parameters of the problem. For instance, it seems intuitive that the magnetic field

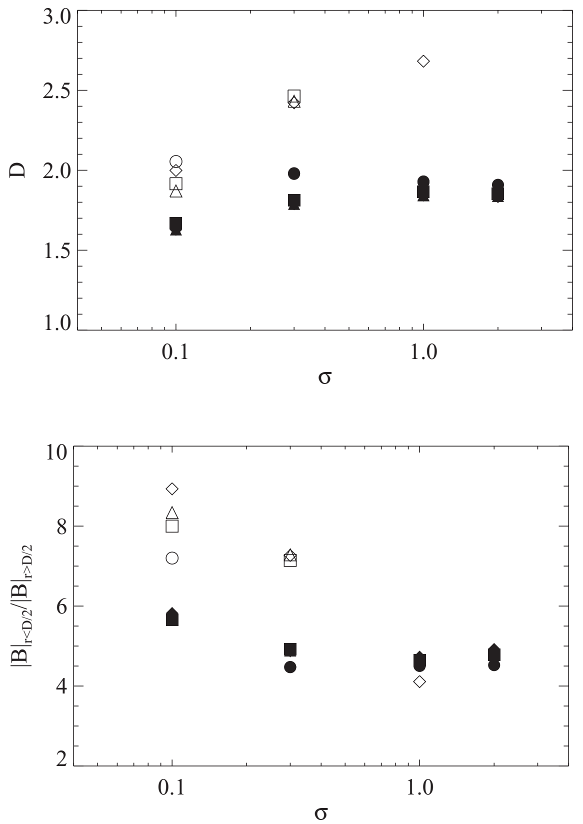

Figure 5. Same quantities as in Fig. 4 but as a function of Prandtl number σ. Here, the different symbols represent rotation rates 0.0 (diamonds), 0.02 (upward triangles), 0.05 (squares) and 0.1 (circles), respectively. Again, open symbols are for resulting converging flows and solid symbols for diverging flows, respectively.

strength would decrease and the size would increase with increasing rotation rate, and this is indeed the case as seen in Fig. 4. Although the changes are not very large, the size D does increase and the field strength ratio decreases in most cases. The dependence on the Prandtl number is shown in Fig. 5. Field strength ratio decreases and structure size increases quite strongly with increasing Prandtl number. It is important to note that in all but one case converging flows produce better confined magnetic structures with smaller D and larger field strength ratio.

For a small number of cases, we have also varied the value of Q which defines how much magnetic flux is in the system. The parameters for these cases are $\Omega = 0, \sigma = 0.03$ and $Q = 8, 16, 32, 64, 128$. All other parameters are the same as in the reference case. With increasing Chandrasekhar number Q, the field strength ratio broadly increases, but the ratio is close to or above 4 only for the highest two values of Q, i.e. a strongly confined magnetic field region is realized.

Lastly, it should be noted that other parameters of the problem can also effect the results, e.g. the Rayleigh number R that governs the strength of the convection. An example in which we increased the strength of the convection compared to the reference case is shown in Fig. 2. There, a converging over diverging flow forms instead of the diverging flow in the reference case. Instead of a single circulation, a weak secondary convective cell is formed in this case further away from the axis. The horizontal size of the magnetic field strength concentration is significantly smaller and the field strength ratio higher than in the reference case.

4 CONCLUSIONS

Our simulations were motivated by the problem of how structures such as magnetic pores or sunspots form at the solar surface and what types of flow are associated with them. The simulations were performed in a restricted, axisymmetric geometry and employ significant simplifications. We therefore have to be careful when trying to draw conclusion for the solar case. Nevertheless, the simulation can provide insight into the mechanisms that are involved in maintaining a tightly concentrated magnetic field in a stratified medium. The quantitative results of this study are effected by all these simplifications as well as by the finite aspect ratio and the boundary conditions chosen. Therefore, our primary interest was the qualitative behaviour, in particular the direction of the flow inside or very close to the flux concentration, i.e. the flow direction of innermost convection cell. Due to the simplicity of these simulations, we were able to explore a range of parameters. The simulations have shown that, depending on the parameters, stable, well-concentrated magnetic structures can exist with both types of flow configurations: an inflow (towards the axis of the flux concentration) above and an outflow deeper below or vice versa. In many of the studied cases, the initial conditions turned out to be important, although such a strong sensitivity to the initial conditions is probably due to the confined geometry and may disappear, e.g. if non-rotationally symmetric disturbances were allowed. But, this does not affect one of the main results of this study which is that, in general, converging flows over diverging flows are associated with more strongly confined magnetic field configuration and the opposite flow configuration. For parameter sets that allowed for both types of solutions, the solution with the converging flow at the top almost always exhibited higher magnetic field strengths and a smaller structure size.

ACKNOWLEDGMENTS

Part of this work was done during the 2010 Summer Program of the Center for Turbulence Research (CTR) at Stanford University. The support provided by CTR is greatly appreciated.

REFERENCES

Botha G. J. J., Rucklidge A. M., Hurlburt N. E., 2006, MNRAS, 369, 1611
Botha G. J. J., Busse F. H., Hurlburt N. E., Rucklidge A. M., 2008, MNRAS, 387, 1445
Hurlburt N. E., Rucklidge A. M., 2000, MNRAS, 314, 793
Hurlburt N. E., Matthews P. C., Proctor M. R. E., 1996, ApJ, 457, 933
Kitiashvili I. N., Kosovichev A. G., Wray A. A., Mansour N. N., 2009, ApJ, 700, L178
Kitiashvili I. N., Kosovichev A. G., Wray A. A., Mansour N. N., 2010, ApJ, 719, 307
Rempel M., 2011, ApJ, 729, 5
Rempel M., Schüssler M., Knölker M., 2009, ApJ, 691, 640
Zhao J., Kosovichev A. G., Sekii T., 2010, ApJ, 708, 304